Pressure effects on the phase separation of $Pr_{0.6}Ca_{0.4}MnO_3$ thin films

2008 J. Phys.: Condens. Matter 20 485202

(http://iopscience.iop.org/0953-8984/20/48/485202)

J. Phys.: Condens. Matter **20** (2008) 485202 (10pp) doi:10.1088/0953-8984/20/48/485202

Pressure effects on the phase separation of $Pr_{0.6}Ca_{0.4}MnO_3$ thin films

A Antonakos[1], D Lampakis[1], E Liarokapis[1], M Filippi[2], W Prellier[2], P Auban-Senzier[3] and C Pasquier[3]

[1] Department of Physics, National Technical University, GR-15780 Athens, Greece
[2] Laboratoire CRISMAT, CNRS UMR 6508, ENSICAEN, 6 Bd Marechal Juin, F-14050 Caen Cedex, France
[3] Laboratoire de Physique des Solides, Universite Paris-Sud, CNRS, UMR 8502, 91405 Orsay, France

E-mail: tantonak@central.ntua.gr

Received 23 May 2008, in final form 12 September 2008
Published 17 October 2008
Online at stacks.iop.org/JPhysCM/20/485202

Abstract

Micro-Raman measurements under high hydrostatic pressures (up to ~6.5 GPa) have been carried out on $Pr_{0.6}Ca_{0.4}MnO_3$ thin film grown on $LaAlO_3$ substrate at room and low temperatures (down to 80 K). We had investigated in detail the temperature and hydrostatic pressure dependence of the Raman phonons and calculated their $\beta = \mathrm{d}\ln\omega/\mathrm{d}p$ values and the Gruneisen parameters. Under the external pressure, certain peaks attributed to metallic phase gain intensity and become narrower. The charge ordered insulating phase, characterized by the orthorhombic-type Jahn–Teller broad band, is suppressed up to a critical pressure $p_{c1} \approx 2$ GPa, and the diffuse electronic scattering intensity decreases, implying that the compound becomes more conductive. However, the pressure is not enough to melt the charge ordered phase, while upon further increase ($p_{c2} \approx 4$ GPa) the macroscopic state remains insulating, at least up to the magnitudes studied. The behaviour of the system is ascribed to the electronic phase separation between a ferromagnetic metallic phase and an antiferromagnetic charge ordered insulating one.

1. Introduction

During the past decades considerable theoretical and experimental research has been carried out on rare-earth manganites with the general formula $R_{1-x}A_xMnO_3$ (R: a trivalent rare-earth ion; A: a divalent alkaline-earth ion) [1], due to their colossal magnetoresistance (CMR) effect [2, 3]. In the doped manganites the mixed valence of the manganese ion can be treated by assuming the coexistence of Mn^{3+} and Mn^{4+} ions in a suitable ratio. The complex physics of the manganites can be described by a Jahn–Teller (JT) induced charge localization competing with the magnetic interactions (double exchange-DE-model [4]) [5]. Therefore, the transport and magnetic properties are affected by internal (doping concentration, average atomic radius $\langle r_A \rangle$) and external perturbations (temperature, pressure, and magnetic field). In the latter case one must take under consideration the strains in thin films from the substrate, which lead to changes in their physical properties [6]. All these variables lead to the complex phase diagram of manganites, which contains several magnetic (ferro—FM, antiferro—AF, para—PM) and charge (metallic—M, insulating—I, charge ordered—CO) phases [7–9].

The compound $Pr_{1-x}Ca_xMnO_3$ (PCMO) is characterized by the absence of size mismatch, i.e., a constant $\langle r_A \rangle$ value ~1.18 Å and shows both hole and electron doping regions [10, 11]. The large size difference between the Pr/Ca and Mn cations leads to a small tolerance factor and a small transfer integral between the Mn atoms in the whole doping range [12]. The e_g electrons are localized and the CO phase occurs at $0.3 \leqslant x \leqslant 0.75$ for $T \leqslant T_{CO}(x)$, where 220 K $\leqslant T_{CO}(x) \leqslant$ 260 K, depending on the amount of Ca doping (x). The compound remains a paramagnetic insulator for all Ca doping levels at zero applied magnetic field. It is a common opinion that PCMO samples are always phase separated and in particular for $0.3 \leqslant x \leqslant 0.5$, the ferromagnetic metallic regions coexist with the antiferromagnetic and charge ordered ones [13–20]. Within the CO phase, there is a magnetic transition to an AFI phase at temperature $T_N < T_{CO}$. Across the CO transition, where the carriers become strongly localized, strong electron–phonon (e–ph) interactions induce

structural changes in the compound. The CO phase is sensitive to external perturbations such as magnetic [21] or electric fields [22], external pressure [23, 24], and the irradiation by x-rays [25, 26] or visible light [27, 28]. All these perturbations can destroy the CO phase and lead to a more conductive state and to an insulator to metal (IM) transition. The phase separation phenomenon is regarded as an important factor for the large resistivity change accompanied by the first order IM transition [29]. In addition, it was found that the critical magnetic field necessary to destroy CO is greatly reduced when the compound is made in the form of a thin film [6].

An unusual FMI state has been detected for PCMO($x = 0.5$)/LAO thin films [30]. This phenomenon has been explained by assuming an electronic phase separation with the coexistence of an FM phase (observed in the magnetization measurements) and a nonmetallic modulated phase (observed in electron microscopy). In order to explain the resistivity results, it has been speculated that the metallic phase does not percolate. Under pressure the CO phase is expected to melt and a metallic state is induced [23, 24]. The IM transition temperature increases with pressure below a critical pressure p^* [24]. Above this p^* the material returns to the insulating state. When x is near 0.5 the CO is more robust and the required pressure for the IM transition is increased. The CO state is optimized at $x = 0.5$, where the carriers are exactly commensurate with the 1:1 ordering of the Mn^{3+}:Mn^{4+} ions.

There are some hydrostatic pressure Raman studies on certain manganites [32, 34, 31, 33, 35] but not many on the less studied PCMO system. Raman scattering in PCMO compounds reveals that the strong coupling between spin and charges induces variations in the mode frequencies and line-widths of the tilting A_g (2) and A_g (4) phonons [36–39], while the intensities of the JT modes increase rapidly within the CO phase [38–40]. In a previous Raman study of $Pr_{0.5}Ca_{0.5}MnO_3$ (PCMO) thin films of 180 nm thickness [38], the modifications in the Raman spectra due to the charge ordering when temperature and hydrostatic pressure are varied were pointed out.

In the present work, a systematic study of the pressure dependence of the Raman active phonons in the range 1 bar–6.5 GPa is presented and combined with low temperature measurements to investigate the effect of pressure on the phase separation and the IM transition. As found by theoretical and experimental investigations [41–43], the signature of the IM transition can be identified by a significant narrowing of the line-width, the hardening of the frequency of the modes related with the stretching or bending of the octahedra, and the decreased intensity of the diffuse electronic scattering. These effects are direct consequences of the reduction of the lattice coupling to the carriers and the increased screening in the metallic phase. Therefore, Raman spectroscopy is an excellent tool, especially for high pressure studies on these materials.

2. Experimental details

Films of $Pr_{0.6}Ca_{0.4}MnO_3$ (PCMO) were deposited on $LaAlO_3$ (LAO) substrate. The films were grown *in situ* using pulsed laser deposition (PLD) and had a thickness of 150 nm. A more detailed analysis of the growth procedure is described elsewhere [30, 44, 45]. X-ray diffraction (XRD) studies have shown that the films were single crystals, while according to transmission electronic microscopy (TEM) measurements the samples are homogeneous. It has been found that the films were [101] oriented on the LAO substrate as a result of the lattice mismatch between film and substrate [44]. Using the XRD results, the out-of-plane lattice parameter of the substrates was calculated to be 3.89 Å, confirming that the film is under a 2.6% compressive strain on LAO. The structure of bulk $Pr_{0.5}Ca_{0.5}MnO_3$ is orthorhombic ($Pnma$) with lattice constants $a = 5.395$ Å, $b = 7.612$ Å and $c = 5.403$ Å [46].

The Raman spectra were obtained using a T64000 Jobin Yvon triple spectrometer, equipped with a liquid nitrogen cooled charge coupled device (CCD) and a microscope. The 514.5 nm line of an Ar^+ laser was used for excitation at low power, which was kept fixed during the measurements at the level of ∼0.2 mW on the surface of the film. The spectral resolution was less than 1 cm^{-1} as checked by the 871.74 nm line of a fluoride lamp. Raman spectra of the film were measured at a temperature region from 78 to 295 K. A backscattering geometry was used, with the sample placed under the microscope with 100× magnification. For the low temperature measurements, an open-cycle Oxford cryostat (Microstat^{He}) was used. The temperature instability was less than 1 K and the local heating due to the laser beam was estimated to be less than 10 K [47, 48]. Several points of the surface have been studied in order to check the homogeneity of the films and the reproducibility. This surface scanning confirmed that the films are homogeneous.

A Merrill–Bassett type diamond anvil cell (DAC) [49], equipped with type one diamonds suitable for optical measurements, was used for the high pressure measurements, which allowed the Raman studies to be carried out in a backscattering geometry. Low temperature measurements were carried out in a quasi-hydrostatic environment from 80 K to room temperature (RT) by incorporating the small DAC into the cryostat. The DAC was fixed into the cryostat cold finger with vacuum glue. The pressure-transmitting medium was a mixture of methanol–ethanol (4:1) [50]. In this set-up the pressure could not be kept fixed at LT increasing by decreasing temperature. By including several small silicon crystals inside and outside the DAC and the cryostat the effect of pressure could be discriminated from that induced by the low temperature or any misalignment of the spectrometer during the measurement. In addition, the pressure was calibrated and the hydrostatic environment was continuously inspected by checking the Si line at 520.5 cm^{-1} for all Si crystals in the DAC. The least square fit of the Si line versus pressure, as proposed by Weinstein and Piermarini [50], is $\Delta\omega = (0.52 \pm 0.03\ cm^{-1}\ kbar^{-1})p + (-0.007 \pm 0.0002\ cm^{-1}\ kbar^{-2})p^2$. The possibility of a local heating of the samples by the applied laser beam was excluded by testing the variation of the spectra for various power densities. Accumulation times were of the order of 2–6 h. During the long accumulations the stability was checked regularly, and especially, at low temperatures or high pressures we check every 15 min and if necessary correct.

3. Results

The orthorhombic $PrMnO_3$ is structurally distorted with respect to the cubic perovskite in two ways: the MnO_6 octahedra present a strong JT cooperative distortion due to Mn^{3+} ions, and the octahedra are tilted in order to optimize the R–O bond lengths [51]. $CaMnO_3$ also has the orthorhombic structure but the Jahn–Teller distortion is negligible. The *Pnma* structure of the compound (point group symmetry D_{2h}) gives $7A_g + 5B_{1g} + 7B_{2g} + 5B_{3g}$ Raman active zone-centre optical phonons [52]. As Ca doping increases, the Jahn–Teller distortion decreases as a consequence of the introduction of Mn^{4+} cations, and the structure becomes more regular, maintaining the tilting of the octahedra. The partial substitution of Pr by Ca is expected to induce phonon broadening from the disorder and the relaxation of the $q \simeq 0$ rule in the light scattering. In general, there are several different contributions to the Raman spectra of manganites; first order (R_{ph}), second order and/or other contributions (such as peaks on the phonon density of states (PDS) or van Hove singularities) from nonzero q points, and electronic scattering (R_{el}) [43]. No contributions from nonzero q points have been observed in the studied spectral region. R_{ph} follows selection rules while the second order scattering and the phonon density of states (PDS) contributions exhibit broad bands. R_{el} is the diffuse continuum scattering and contributes to the Raman background and intensity. The Raman spectrum $R(\omega)$ can be fitted and mathematically expressed by the equation [43]:

$$R(\omega) = R_{ph} + R_{el},$$

where

$$R_{ph} = [1 + n(\omega)] \sum_{(i=1)}^{n} (A_i \omega \Gamma_i)/((\omega^2 - \omega_{i^2})^2 + \omega^2 \Gamma_i^2),$$

represents the phonon modes with associated phonon frequency ω_i, line-width Γ_i and amplitude A_i, and

$$R_{el} = [1 + n(\omega)][(A\omega/\tau)/(\omega^2 + (1/\tau)^2)]$$

is the R_{el} contribution to the spectrum consisting of a low frequency response associated with the diffusive hopping of the carriers with the scattering rate $\gamma = 1/\tau$. The quantity $[1 + n(\omega)] = [1 - \exp(-\omega/kBT)]^{-1}$ is the Bose–Einstein thermal factor. The R_{el} contribution was fitted by a split Lorentzian and was subtracted from the collected spectrum to obtain the R_{ph}. Yoon *et al* [43] have shown that when the compound is an insulator the R_{el} can be fitted as an exponential background. The intensity of the R_{el} scattering decreases considerably close to the IM transition, and when the metallic state is fully established only a constant continuum contributes to the Raman spectra [43]. For the assignment of the R_{ph} spectra we collected spectra at several polarizations. However, the crossed polarization measurements were of poor statistics and time consuming (more than 7 h). We observed the same modes with [38] and [39], where detail assignment of the modes is done, and since they seem to follow the same selection rules, we follow the same mode assignment.

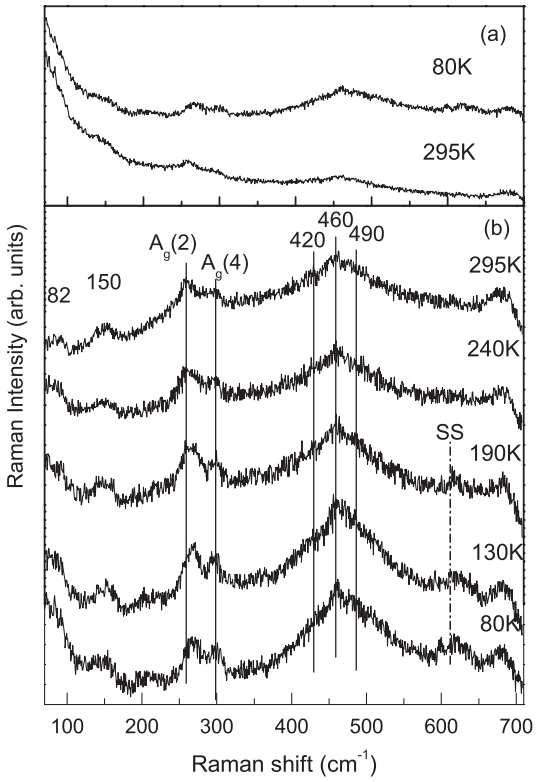

Figure 1. (a) Typical Raman spectra at 80 K and room temperature. The R_{el} strongly contributes to the spectra even at 80 K. (b) The R_{ph} spectra at selected temperatures for the PCMO/LAO thin film in parallel backscattering polarization geometry using the 514.5 nm excitation wavelength.

In figure 1(a) typical Raman spectra of the PCMO film are shown at 80 K and RT for comparison of the R_{el} scattering. Even at 80 K there is a strong contribution from the electronic scattering. This according to Yoon *et al* indicates that the compound remains an insulator [43]. Figure 1(b) presents the R_{ph} spectra for the temperature range 78–295 K. Table 1 summarizes the observed bands with their assignment and pressure characteristics. The low frequency bands are attributed to R–O modes and correspond to mixed R and O1 vibrations within the xz plane (A_g and B_{2g} symmetry modes) and around the y axes (B_{1g} and B_{3g} modes) [52]. The ∼260 cm^{-1} mode was attributed to the $A_g(2)$ soft mode, which is related with the tilting angle of the MnO_6 octahedra. The neighbouring peak at ∼300 cm^{-1} is assigned to the $A_g(4)$ tilting mode. In the 400–500 cm^{-1} bending region the spectra consist of at least three bands. With increasing Ca doping the JT distortion is reduced and these subbands are better distinguished [39, 40]. The ∼480 cm^{-1} peak of B_{2g} symmetry couples with the CO state [38] and is assigned to a mixed bending and antisymmetric ($B + AS$) JT mode [39, 53]. The ∼618 cm^{-1} mode of A_g symmetry gains intensity with decreasing temperature, it couples with the CO phase, and it is attributed to the symmetric stretching JT mode (SS). The 675 cm^{-1} mode of A_g symmetry is assigned to the lattice–substrate interaction [39, 54].

Figure 2 presents typical room temperature Raman spectra of the PCMO film at selected hydrostatic pressures up to

Table 1. Observed modes on PCMO($x = 0.4$), their assignments, $d\omega/dp$, β, γ_i, $d\omega/dT$ (at ambient pressure) and $(d\omega/dT)_p = 3.5$ GPa (the $d\omega/dT$ values under the average 3.5 GPa pressure).

Energy (cm^{-1})	Symmetry	Assignment	$d\omega/dp$ (cm^{-1} GPa^{-1})	$\beta_i = d\ln\omega_i/dp$	γ_i	$d\omega/dT$ (cm^{-1} K^{-1})	$(d\omega/dT)_{p\approx3.5\ GPa}$ (cm^{-1} K^{-1})$_P$
81	A_g	$R(x)$					
148	Broad						
[143	[B_{2g}	[$R(y)$					
153]	B_{1g}/B_{3g}]	$R(z)$]					
210	A_g	$R(x)$				0.03	
268	A_g	$A_g(2)$ tilting mode	1.07	0.004	1.08	−0.039	−0.05
300	A_g	$A_g(4)$ tilting mode	1.31	0.0039	1.188	−0.014	−0.05 (<190: 0.04)
350		IR band ?/ IM transition				0.04 ± 1	0.1 ± 0.06
425	B_{2g}	Bending	1.33	0.003	0.81	−0.2	−0.26
460	B_{1g}/B_{3g}	Bending	2.14	0.0037	1	−0.012	−0.01657
490	B_{2g}	Mixed $B + AS$ JT	1.41	0.003	0.81	−0.0378	−0.0314
580	A_g	JT-like					0.0047
618	A_g	JT SS				0.004	0.0047
675	A_g	Lattice–substrate interaction				−0.012	

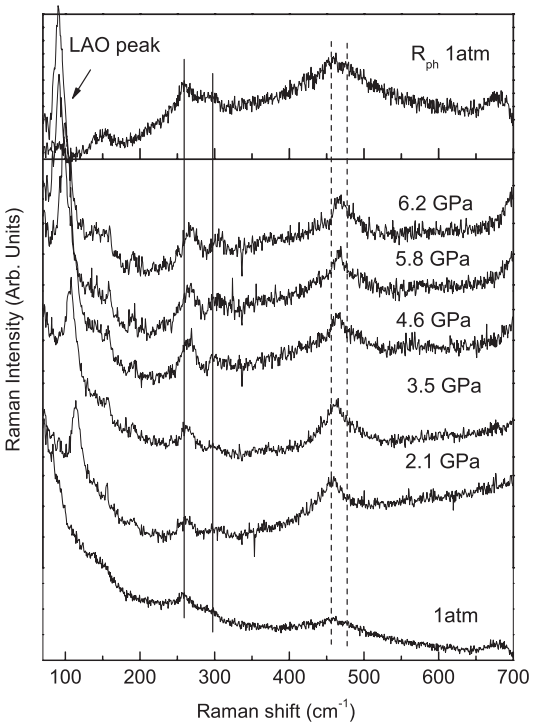

Figure 2. Typical Raman spectra at selected different hydrostatic pressures measured on the PCMO/LAO thin film in parallel backscattering polarization geometry using the 514.5 nm laser line. For the 1 atm spectrum the R_{el} dominates over the R_{ph} contribution, which is presented in the upper layer.

6.2 GPa. At low frequencies, the LAO peak at ∼120 cm^{-1} is observed when introducing a small piece of the PCMO thin film in the DAC. In this configuration the substrate contributes slightly to each spectrum. The intensity of the R_{el} decreases considerably under a pressure of 2.1 GPa. The two tilting phonons at ∼260 and ∼300 cm^{-1} are observed, which are better distinguished above 2 GPa due to their increased intensity and the reduction of the ∼260 cm^{-1} phonon line-width (full-width at half-maximum—FWHM). In the bending region pressure induces changes in the subbands of the broad feature. The fitting of the spectra has been carried out by using Lorentzian peaks and the results are shown in figure 3. As can be seen, the frequency of the $A_g(2)$ mode at ∼260 cm^{-1} increases almost linearly with pressure, while its line-width decreases rapidly and for pressures above ∼2 GPa remains practically constant (figure 3(a)). In figure 3(b) it can be seen that the frequency of the $A_g(4)$ mode at ∼300 cm^{-1} increases slightly for pressures between ∼2 and 4 GPa and rapidly at low pressures (<2 GPa) or above ∼4.5 GPa. Since this mode is relatively weak, no conclusive results can be obtained concerning its line-width, which however seems to remain constant with pressure (figure 3(b)).

The 400–500 cm^{-1} bending region was firstly fitted by one broad Lorentzian. Figure 3(c) shows that the frequency of this broad feature located around 460 cm^{-1} increases almost linearly with pressure above 2 GPa. However, the bending region consists of three subbands. The parameters from the fitting analysis of the broad feature to its three subbands (the ∼430 cm^{-1} B_{2g} mode, the ∼460 cm^{-1} bending mode, and the JT AS mode) are presented in figure 4. We observe abrupt changes in their line-widths and the three subbands appear narrower above 2 GPa. This explains why the broad band loses weight from the higher frequency side, where the JT AS occurs. Concerning their frequencies the large error bars do not allow us to draw any conclusions.

Figure 5 presents high pressure (2.6–4.4 GPa) micro-Raman spectra acquired in the temperature range 80–295 K. Compared to low temperatures ambient pressure, the R_{el} intensity is decreased and a broad band at ∼350 cm^{-1} is observed, more clearly for $T < 190$ and $p = 3.7$ GPa. In addition, while at ambient pressure the JT AS mode contributes

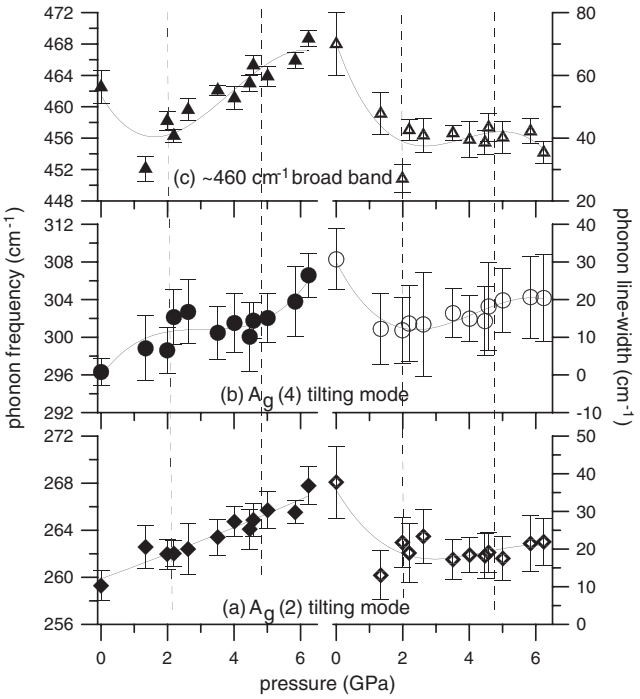

Figure 3. The hydrostatic pressure dependence of the frequency (filled symbols) and line-width (FWHM, grey open symbols) of (a) the $A_g(2)$ mode at ∼268 cm^{-1}, (b) the $A_g(4)$ mode at ∼300 cm^{-1}, and (c) the average wide band at ∼460 cm^{-1}. However, the bending region consists of three subbands. The parameters from the fitting analysis of the broad feature to its three subbands are presented in figure 4. The continuous lines are the polynomial fitting of the symbols using the error bars as weight.

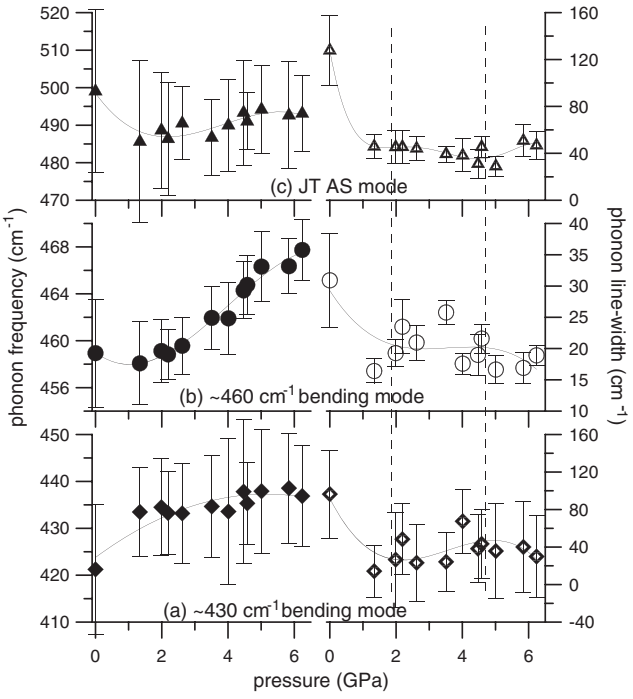

Figure 4. The hydrostatic pressure dependence of the frequency (filled symbols) and line-width (FWHM, grey open symbols) of (a) the B_{2g} mode at ∼430 cm^{-1}, (b) the B_{1g} (or B_{3g}) mode at ∼460 cm^{-1}, and (c) the JT AS mode at ∼490 cm^{-1}, which constitute the broad feature at the bending region. The continuous lines are the polynomial fitting of the symbols using the error bars as weight.

to the asymmetry of the broad feature at 400–500 cm^{-1}, at high pressures both the ∼460 cm^{-1} bending mode and the JT AS mode are clearly distinguished. This is related with the decreased JT distortion. The JT SS mode at ∼618 cm^{-1} does not appear. Instead a mode at ∼580 cm^{-1} appears with a similar symmetry and behaviour. A JT-like mode has been also observed in PCMO($x = 0.6$)/LAO thin films, where the JT SS mode weakens and the CO phase is reduced [39, 40].

Figure 6 presents the temperature variation of the frequency and line-width of the two A_g tilting modes at ∼260 cm^{-1} and ∼300 cm^{-1} as well as of the broad peak at ∼350 cm^{-1} in the pressure range 2.6–4.4 GPa and at ambient pressure. As observed before in the temperature-dependent results, the fitting errors are higher than the ones of the high pressure measurements [31]. At ambient pressure the frequency of the $A_g(2)$ mode shows an almost linear increase with decreasing temperature while its line-width decreases. At high pressures, although its frequency shows similar behaviour, its line-width remains practically constant but narrower than at ambient pressure. Concerning the $A_g(4)$ mode, its frequency shows an abnormal behaviour with a maximum around 125 K. The data for the line-width are not good enough to draw any conclusions. Finally, the frequency of the ∼350 cm^{-1} seems to decrease at low temperatures and high pressures contrary to the ambient pressure low temperature behaviour. Although this mode is mainly observed under pressure and low temperatures ($T < 190$ K, $p > 3.7$ GPa), the fitting procedure requires its presence as a weak peak even at RT. At ambient pressure it is very weak even at low temperatures but again it is necessary for an appropriate fitting analysis. The line-width of this broad mode does not seem to be affected by the temperature and pressure variations.

Figure 7 presents the temperature variation at ambient (filled symbols) and high pressures (open grey symbols) of the frequency and line-width of the modes at ∼430, 460, ∼490, and 618 cm^{-1} (associated with the ∼580 cm^{-1} JT-like mode at high pressures). The frequencies of the ∼430 cm^{-1} and the JT AS mode increase slightly at low temperatures. The ∼430 cm^{-1} mode is always greater at high pressures than at ambient, while the JT AS mode is fairly constant. The frequency of the ∼460 cm^{-1} mode increases slightly with decreasing temperature at both ambient and high pressure. The ∼460 cm^{-1} and the JT AS modes are significantly narrower at high pressures at all temperatures, while the ∼430 cm^{-1} mode is fairly constant. The JT SS mode softens across T_{CO} ($p = 0$), it is almost absent at RT (figure 1) although the fitting analysis requires its presence, and gains intensity for $T < T_{CO}$. The intensity of the JT-like mode at ∼580 cm^{-1}, which appear under pressure when the JT SS mode disappears, has similar behaviour but its frequency is constant within experimental error. No significant changes have been observed concerning their line-width.

Most of the observed bands must be attributed to phonons, as they are consistent with other published theoretical and experimental works on manganites. However, the 0.4 Ca

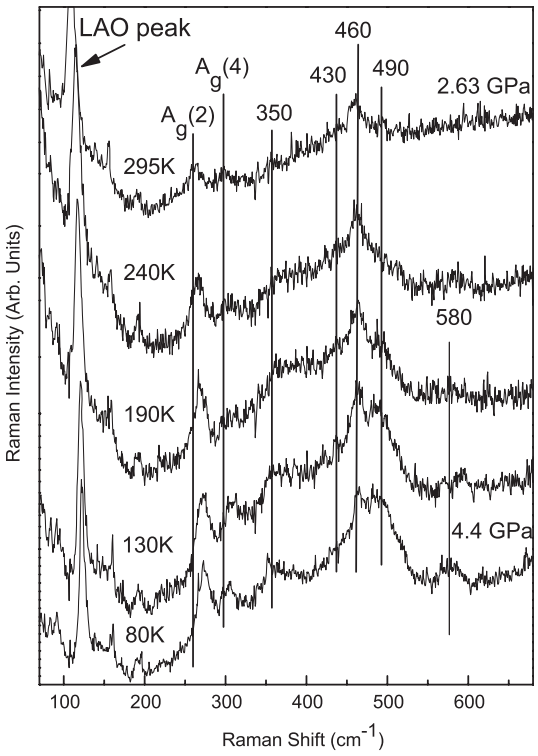

Figure 5. Typical high pressure Raman spectra of the PCMO film in the temperature range 80–295 K and in parallel backscattering polarization geometry, using the 514.5 nm excitation wavelength. The R_{el} contributes to the spectra even at 80 K but it is reduced below 190 K and considerably decreased compared to the ambient pressure low temperature spectra. The pressure increases from 2.65 to 4.4 GPa at lowering temperature from RT to 80 K.

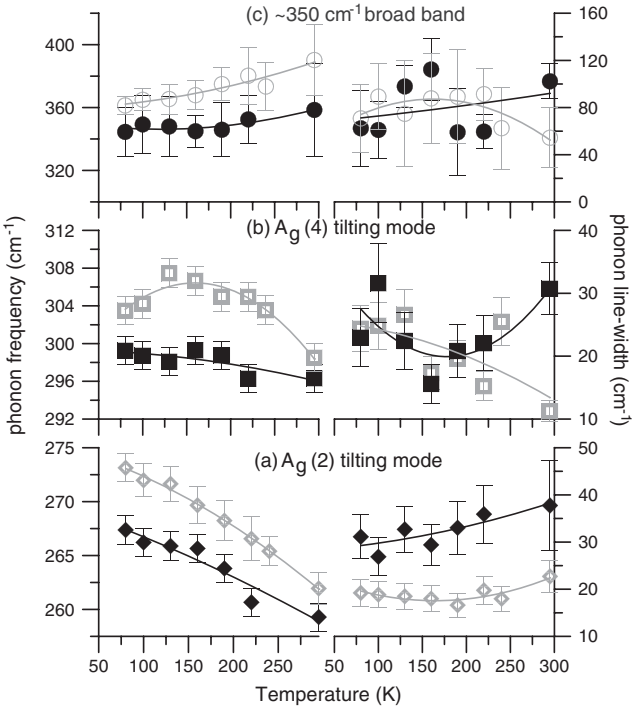

Figure 6. Temperature dependence of the frequency and line-width (FWHM) for the modes observed in the low frequency part of the Raman spectra of the PCMO film obtained at ambient (filled symbols) and high pressure (grey open symbols, an average pressure of 3.5 GPa is assumed). The continuous lines are the polynomial fitting of the symbols using the error bars as weight.

doping and the inhomogeneities on the reduction of the JT octahedra upon pressure can induce, as already mentioned, contributions from nonzero points of the Brillouin zone. These distortions differentiate the spectra from the end compounds; although the rhombohedral-like peaks gain intensity and become narrower upon pressure, they are still broader than in the $CaMnO_3$. In addition, the appearance of the 350 cm^{-1} has been correlated with a symmetry change at LT [62] while the appearance of the JT-like 580 cm^{-1} band is probably correlated with the distorted structure of the compound.

4. Discussion

From the high pressure data at RT we observe that all modes show an abrupt frequency change close to 2 GPa (figures 3 and 4). In some recent suggestions [24, 32, 55], changes are expected above this pressure because the effects are far more complicated than in the low pressure measurements. Above 2 GPa, the pressure dependence of all modes at RT shows a systematic hardening on increasing pressure, as expected from the lattice compression (figures 3 and 4 as a function of pressure and $p > 2$ GPa). As already mentioned, the $A_g(4)$ mode remains almost constant in the 2–4.5 GPa region. Above $p \approx 4$ GPa there is also a change in the slope of the $A_g(4)$ mode and the broad bending region band (figure 3), implying a second critical pressure (p_{c2}).

Table 1 presents the rate of the average $d\omega/dp$ value for all modes. The bending modes involve modifications of the Mn–O–Mn angle and stretching of the R–O(1) bond length [51]. Therefore, their behaviour can be understood as a measure of the compressibility of the R–O(1) bonds [33]. The stretching modes force constants depend on the interatomic distances and the observed modifications can be ascribed to a symmetrization of the MnO_6 octahedra and the reduction of the JT distortion, providing a measure of the compressibility of the Mn–O bonds [33]. In addition, it has been shown for the PCMO films that the JT modes couple with the CO phase [38]. As mentioned above, the $A_g(2)$ and $A_g(4)$ modes correspond to the tilting rotation of the octahedra (around the *b*- and *a*-axes respectively) [52] and couple to the carriers. Therefore, comparing the relative frequency change of each mode, we can observe that: (a) the tilting modes have similar average rate $\beta = d\ln\omega/dp$. (b) The tilting modes have identical β values (table 1) with the $PrMnO_3$ compound [33]. However, the β values are larger than in $PrMnO_3$ for the bending modes and lower for the JT AS mode (0.0026 and 0.0045 respectively for the $PrMnO_3$ [33]). This is related with the Ca ($x = 0.4$) doping because the doped compound has decreased JT distortion and different tilting angle; as shown in [33], differences on the JT distortion and the tilting angle will result in a different pressure dependence of the phonons even for compounds with the same structure. For the films of the present study, a larger change in the stretching mode than in the bending mode indicates a larger compressibility of the Mn–O bonds than the Pr–O bonds.

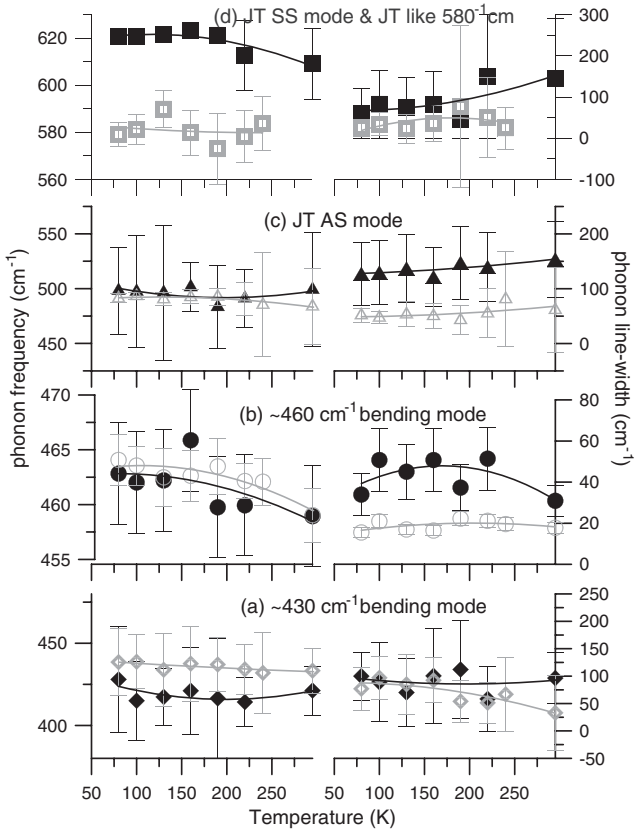

Figure 7. Temperature dependence of the frequency and line-width (FWHM) for the modes observed in the high frequency part of the Raman spectra of the PCMO film obtained at ambient (filled symbols) and high pressure (grey open symbols, an average pressure of 3.5 GPa is assumed). The continuous lines are the polynomial fitting of the symbols using the error bars as weight.

For PCMO($x = 0.5$)/STO quite different $\mathrm{d}\omega/\mathrm{d}p$ values (2.1 cm^{-1} GPa^{-1} for $A_g(2)$ and 5.9 cm^{-1} GPa^{-1} for the broad band at 460 cm^{-1}) have been reported [38]. These differences are due to the different JT amounts and the varying strains. As doping increases from $x = 0.4$ to 0.5 the compressibility for the bulk compound in the cubic approximation decreases from 0.0037 to 0.0033 GPa^{-1} [56]. In addition, the STO substrate has bigger compressibility value than LAO (0.0057 [57] to 0.0052 GPa^{-1} respectively [58]). Then, the difference on compressibility between film and substrate is smaller on the PCMO($x = 0.4$)/LAO than on PCMO($x = 0.5$)/STO. Therefore, an additional pressure effect from this difference in the film–substrate compressibilities must be taken under consideration in the two systems. Since the substrate has a greater compressibility than the film, the film is more sensitive to pressure than the substrate and this pressure effect will be an additional tensile strain in each film. This will result in a greater tensile strain under pressure in the case of the PCMO($x = 0.5$)/STO, while in PCMO($x = 0.4$)/LAO the compressive strain reduces or can even change to a tensile one, as the additional tensile strain activates under pressure. This explains the greater pressure effect on the modes of PCMO($x = 0.5$)/STO [38].

Using the values of the bulk modulus found in [56] (∼270 GPa), we can estimate the Gruneisen parameters, γ_i, which measure the relative change of the mode with volume $\gamma_i = B(\partial \ln\omega_i/\partial p)$, where B is the Bulk modulus. Table 1 lists the γ_i parameters for all modes. It is worth mentioning that values of $\gamma > 1$ and $\leqslant 1$ would be expected for internal and external modes respectively. This is not the case however. This can be explained by the additional previously mentioned pressure-induced tensile strain and by a pressure-induced phase separation scenario, which will be discussed in detail below. Using Monte Carlo simulations it has been shown that the compressibility grows as the phase separated regime is approached [8]. From the analysis of the Monte Carlo configurations it is clear that coexisting clusters with FM and AF properties are generated, where their dynamical coexistence is characteristic of regions with high compressibility [8]. In the present thin films there must be strong charge fluctuations with pressure, since the competing phases have different electronic densities [30]. Therefore, the differences from the expected γ values could originate from the phase separation process. However, further high pressure studies on phase separated systems are required to address this speculation.

Concerning the phonon line-widths (Γ), it is worth mentioning that the phonon lifetimes ($1/\Gamma$) are determined by the decay channels associated with their interactions (e.g. electron–phonon coupling, anharmonicity) [34, 59, 60]. Therefore, the suppression or even a remarkable weakening of a temperature-dependent interaction would reflect the $\Gamma(T)$ dependence. In addition, several pressure-induced effects can affect the $\Gamma(p)$. It is generally accepted that a pressure-induced IM transition should directly reflect the narrowing of the phonon line-width [34, 31]. Therefore, the abrupt narrowing of all modes in the range 0–2 GPa (figures 3 and 4) implies that the compound became more conductive. This assumption is reinforced by the abrupt decrease of the R_{el} intensity upon pressure between the 1 atm and 2.1 GPa spectra (figure 2). However, according to [43], since the R_{el} still contributes as an exponential background to the low frequency part of the spectra the compound appears to retain its semiconducting behaviour.

In figures 6 and 7 we present the low temperature data at ambient pressure and under high pressures. Since the pressure increases from 2.65 to 4.4 GPa on lowering temperature from RT to 80 K, respectively, an average pressure ∼3.5 GPa can be assumed. As table 1 shows, the values of the average $\mathrm{d}\omega/\mathrm{d}T$ are similar for all modes at ambient and under pressure conditions, except for the tilting modes where there is a considerable difference. This is related to the anharmonic behaviour of the tilting modes and it is strong evidence that the pure anharmonic explicit term is important, as was suggested for the PCMO($x = 0.5$)/STO thin films [38]. While the amount of pure anharmonicity is strong for the external vibrational phonons, the explicit anharmonic term is small for the internal modes. It is also important to mention that while the temperature dependence of the $A_g(4)$ phonon frequency is small, the mode shifts strongly with hydrostatic pressure (table 1); its explicit anharmonic term $(\mathrm{d}\omega/\mathrm{d}T)_V$ [38] is larger than in the $A_g(2)$ mode. A remarkable difference is also observed in the $\mathrm{d}\omega/\mathrm{d}T$ values of the 350 cm^{-1} peak (table 1).

Unfortunately, this mode is very weak or absent at ambient pressure and it is only induced by the fitting analysis, so its error bars are too large to allow definite conclusions (table 1).

The $A_g(4)$ phonon shows an additional difference in slope for $T < 190$ K and $p > 3.7$ GPa (figure 6). At this temperature and pressure, the ∼580 cm^{-1} JT-like and the 350 cm^{-1} modes appear, while the JT AS mode is better defined. It is worth mentioning that the appearance of the 350 cm^{-1} mode was also reported across the IM transition for the $La_{0.5}C_{0.5}MnO_3$ compound [61]. Its appearance was related to a symmetry change, which accompanies the IM transition [62, 63]. In addition, while the JT modes lose intensity under pressure, all other peaks gain intensity. Due to these pressure effects, the subbands of the bending region become clearly distinguished at low temperatures and high pressures and reinforce our assumption about the existence of the ∼420 cm^{-1} and ∼490 cm^{-1} bands on the bending region at RT. As we already mentioned the JT modes couple with the CO phase. Especially the JT SS mode increases rapidly below T_{CO} at ambient pressure [38]. However with the application of pressure its intensity decreases implying a suppressed CO phase. The suppressed CO phase has been the main reason in the bulk compound for an induced FMM phase [24]. Finally, the R_{el} intensity is decreased as compared to the ambient pressure LT measurements, also implying that the compound is close to an IM transition. Recent resistivity measurements confirmed that macroscopically the system remains an insulator up to 3 GPa. However, there was a considerable decrease of resistivity on increasing pressure from 2.5 to 3.4 GPa, as the above changes in the Raman spectra indicate.

In order to investigate the el–ph reduction, the JT distortion amplitude, and the possible phase separation scenario, it is worth looking at the relative intensities of the modes at RT. In particular, figure 8 presents the pressure dependence of the relative intensities of the JT AS mode to the $A_g(2)$, $A_g(4)$, and the ∼460 cm^{-1} B_{1g} bending mode at RT. As can be seen, the JT AS mode loses intensity with respect to the $A_g(2)$, $A_g(4)$, and 460 cm^{-1} bending modes from 0 to 3 GPa (figures 8(a)–(c)) indicating a decrease of the JT distortion. The reduction of the JT distortion weakens the el–ph interaction inducing a charge delocalization [64]. The tilting and bending peaks are attributed to the metallic rhombohedral-like phase [51]. The reduction of the JT distortion may cause the enhancement of the double exchange mechanism and in turn make the sample more conductive. The increased intensity and the reduced line-width of the 'metallic' peaks is similar to the changes induced from the chemical pressure (Ca substitution) and it is attributed to FMM clusters formed in the insulating phase, which is characterized by the JT broad bands [51]. The insulating phase decreases rapidly with increasing pressure up to the critical value $p^* \sim 4.5$ GPa. On the contrary, the FMM phase (identified by the sharp rhombohedral-like peaks) increases. Figure 8(d) presents the resistivity measurements up to pressures of ∼3 GPa at room temperature. It can be observed that the continuous lines in figures 8(a)–(c) have the same behaviour as the fitted curve of resistivity from figure 8(d). Therefore, the trend of the

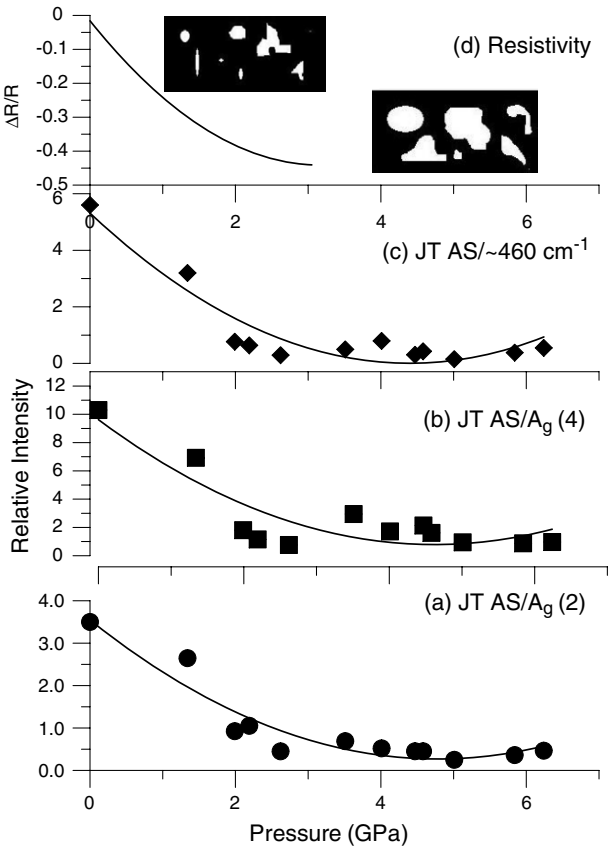

Figure 8. Pressure dependence of the relative intensities of the JT mode to the (a) $A_g(2)$, (b) $A_g(4)$ and (c) 460 cm^{-1} rhombohedral-like modes observed in the Raman spectra of the PCMO film obtained at room temperature. The resistivity results in the region 0–3 GPa are shown on (d). Schematic insets are used to describe qualitatively the phase separation scenario; for $p = 0$ small FMM clusters (white regions) are formed on the insulating phase (black matrix), while at $p = 4.5$ GPa larger FMM clusters are formed and the compound is more conductive. However, the system does not cross the percolation limit.

reduction of the resistivity correlates well with the competition of the two phases as induced by the relative intensity of the corresponding modes in the Raman spectra. It appears that pressure-induced phase competition leads to the rapid decrease of the resistivity as the ferromagnetic metallic phase dominates over the insulating one at $p = 0$–3 GPa. It has been found that a pressure of 2.5 GPa corresponds to a decrease in resistivity of about 40%. This supports the above discussion of the narrower $\Gamma(p)$ from the reduced el–ph interaction.

A phase separation scenario where FMM domains coexist with the COI state gives a good description why we did not detect a metallic phase (at least until 3.4 GPa), although the compound becomes more conductive. As already mentioned, a similar unusual FMI state has been detected for PCMO($x = 0.5$)/LAO thin films [30] and during the production procedure evidenced in the films of the present study [65]. From the trend of the Raman relative intensities, one can speculate that the resistivity does not continue to change above $p_{c2} \approx 4$ GPa. Above p_{c2} (where there is also a slight change in the slope of certain modes), the insulating phase increases slowly, while

the metallic one decreases. Since, we have not observed any IM transition at RT, it is reasonable to assume that for $p > 2$ GPa the compound remains insulating although the ferromagnetic phase appears more intense. This is a similar behaviour to the one observed for bulk PCMO($x = 0.25, 0.3, 0.35$), where an insulating phase with an unknown conducting mechanism appeared and a dynamic JT distortion in the phase was speculated upon [24]. In the same work a critical pressure p^* has been reported, above which the material returns progressively to the insulating state as at ambient pressure. Therefore, the electronic phase separation scenario (with two critical points at $p_{c1} \approx 2$ GPa and $p_{c2} \approx 4$ GPa) seems to describe well all the observations of the Raman spectra on the microscopic level and satisfies the macroscopic resistivity results. This phase separation is schematically presented in figure 8(d). At ambient pressure there is an AFI/CO phase (black matrix) with small FMM clusters (white regions). The increased pressure suppresses the CO phase leading to a more conductive behaviour, which can be described with a phase separation with competing phases that leads to larger FMM clusters. The overall behaviour of the system can be described as a ferromagnetic semiconductor.

In a recent study, Kozlenko *et al* [66] proposed that, unlike other half-doped systems with a relatively large $\langle r_A \rangle$, such as $Pr_{0.5}Sr_{0.5}MnO_3$, $Nd_{0.5}Sr_{0.5}MnO_3$, and also $LaMnO_3$ exhibiting pressure-induced metallization, in $La_{0.5}Ca_{0.5}MnO_3$ and other manganites with smaller $\langle r_A \rangle$ and bandwidth the opposite tendency to pressure-induced charge localization occurs, caused by development of monoclinic distortion due to charge and orbital ordering. They also claimed that $Pr_{0.5}Ca_{0.5}MnO_3$ could likely show similar behaviour. Our data indicate that pressure induces a charge delocalization and suppresses the CO phase at RT on PCMO($x = 0.4$)/LAO thin films, while no pressure-induced IM transition has been observed at LT. These results, which are better explained in the phase separation scenario, confirm the complicated physics of the PCMO compound and indicate that this compound should not be included in the two cases, probably due to the absence of $\langle r_A \rangle$ mismatch, its different bandwidth and the CO/AFM insulating ground state.

5. Conclusions

We have studied the pressure-induced effects on the Raman spectra of PCMO($x = 0.4$) thin films grown on LAO substrate. The compressibility of the Mn–O bonds is larger than R–O ones. The pressure has a smaller effect on the PCMO($x = 0.4$)/LAO phonons compared to PCMO($x = 0.5$)/STO thin films as a result of a pressure-induced tensile strain, due to the greater difference in compressibility between the PCMO($x = 0.5$) thin film and the STO substrate. Based on the temperature and hydrostatic pressure dependence of the phonons, we have calculated their $\beta = \mathrm{d}\ln\omega/\mathrm{d}p$ values and the Gruneisen parameters. The amount of anharmonicity between the tilting modes is estimated to be stronger on the $A_g(4)$ mode than on the $A_g(2)$ one. The macroscopic resistivity behaviour is correlated with the relative intensities of the insulating phase broad JT modes to the sharp metallic-like phase peaks. A pressure-induced phase separation scenario where FMM domains coexist with the insulating state gives a good description of the thin film semiconducting behaviour.

Acknowledgments

Work supported through the project ‘Pythagoras I’, co-funded by the European Social Fund (75%) and Greek National Resources (25%) and the project E.C. STREP No 517039 project ‘COMEPHS’.

References

[1] Ramirez A P 1997 *J. Phys.: Condens. Matter* **9** 8171
[2] Jin S, Tiefel H, McCormack M, Ramesh R and Chen L H 1994 *Science* **264** 413
[3] Millis A J 1998 *Nature* **392** 147
Fontcuberta J 1999 *Phys. World* **12** 33
[4] Zener C 1951 *Phys. Rev.* **82** 403
[5] Millis A J, Littlewood P B and Shraiman B I 1995 *Phys. Rev. Lett.* **74** 5144
[6] Prellier W, Lecoeur Ph and Mercey B 2001 *J. Phys.: Condens. Matter* **13** R915
[7] Cheong S-W and Hwang H Y 2000 *Colossal Magneto Resistance Oxides* (*Monograph in Condensed Matter Science*) ed Y Tokura (New York: Gordon and Breach)
[8] Moreo A, Yunoki S and Dagotto E 1999 *Science* B **283** 2034
[9] Moritomo Y, Tomioka Y, Asamitsu A, Tokura Y and Matsui Y 1995 *Phys. Rev.* B **51** 3297
[10] Martin C, Maignan A, Hervieu M and Raveau B 1999 *Phys. Rev.* B **60** 12191
[11] Tokura Y and Tomioka Y 1999 *J. Magn. Magn. Mater.* **200** 1
[12] Tokura Y, Tomioka Y, Kuwahara H, Asamitsu A, Moritomo Y and Kasai M 1996 *J. Appl. Phys.* **79** 5288
[13] Kida N and Tonouchi M 2002 *Phys. Rev.* B **66** 024401
[14] Fisher L M, Kalinov A V, Voloshin I F, Babushkina N A, Kugel K I and Khomskii D I 2003 *Phys. Rev.* B **68** 174403
[15] Mercone S, Wahl A, Pautrat A, Pollet M and Simon C 2004 *Phys. Rev.* B **69** 174433
[16] Kajimoto R, Mochizuki H, Yoshizawa H, Okamoto S and Ishihara S 2004 *Phys. Rev.* B **69** 054433
[17] Padhan P, Prellier W, Simon Ch and Budhani R C 2004 *Phys. Rev.* B **70** 134403
[18] Freitas R S, Mitchel J F and Schiffer P 2005 *Phys. Rev.* B **72** 144429
[19] Dalai M K, Pal P, Sekhar B R, Saini N L, Singhal R K, Garg K B, Doyle B, Nannarone S, Martin C and Studer F 2006 *Phys. Rev.* B **74** 165119
[20] Saurel D, Simon Ch, Brulet A, Heinemann A and Martin C 2007 *Phys. Rev.* B **75** 184442
[21] Tomioka Y, Asamitsu A, Moritomo Y and Tokura Y 1995 *J. Phys. Soc. Japan* **64** 3626
[22] Asamitsu A, Tomioka Y, Kuwahara H and Tokura Y 1997 *Nature* **388** 50
[23] Moritomo Y, Kuwahara H, Tomioka Y and Tokura Y 1997 *Phys. Rev.* B **55** 7549
[24] Cui C and Tyson T A 2004 *Phys. Rev.* B **70** 094409
[25] Cox D E, Radaelli P G, Marezio M and Cheong S W 1998 *Phys. Rev.* B **57** 3305
[26] Kiryukhin V, Casa D, Hill J P, Keimer B, Vigliante A, Tomioka Y and Tokura Y 1997 *Nature* **386** 813
[27] Miyano K, Tanaka T, Tomioka Y and Tokura Y 1997 *Phys. Rev. Lett.* **78** 4257
[28] Mori T, Ogawa K, Yoshida K, Miyano K, Tomioka Y and Tokura Y 1997 *J. Phys. Soc. Japan* **66** 3570

[29] Ghivelder L, Freitas R S, das Virgens M G, Continentino M A, Martinho H, Granja L, Quintero M, Leyva G, Levy P and Parisi F 2004 *Phys. Rev.* B **69** 214414
[30] Haghiri-Gosnet A M, Hervieu M, Simon Ch, Mercey B and Raveau B 2000 *J. Appl. Phys.* **88** 3545
[31] Congeduti A, Postorino P, Caramagno E, Nardone M, Kumar A and Sarma D D 2001 *Phys. Rev. Lett.* **86** 1251
[32] Pinsard-Gaudart L, Rodriguez-Carvajal J, Daoud-Aladine A, Goncharenko I, Medarde M, Smith R I and Revcolevschi A 2001 *Phys. Rev.* B **64** 064426
[33] Martyn-Carron L, Sanchez-Bentez J and de Andres A 2003 *J. Solid State Chem.* **171** 313
[34] Sacchetti A, Dore P, Postorino P and Congeduti A 2004 *J. Phys. Chem. Solids* **65** 1431
[35] Postorino P, Congeduti A, Degiorgi E, Itie J P and Munsch P 2002 *Phys. Rev.* B **65** 224102
[36] Dediu V, Ferdeghini C, Matacotta F C, Nozar P and Ruani G 2000 *Phys. Rev. Lett.* **84** 4489
[37] Gupta R, Venketeswara Pai G, Sood A K, Ramakrishnan T V and Rao C N R 2002 *Europhys. Lett.* **58** 778
[38] Tatsi A, Papadopoulou E l, Lampakis D, Liarokapis E, Prellier W and Mercey B 2003 *Phys. Rev.* B **68** 024432
[39] Antonakos A, Palles D, Liarokapis E, Filippi M and Prellier W 2008 *J. Appl. Phys.* **104** 063508
[40] Antonakos A, Lampakis D, Palles D, Liarokapis E, Prellier W and Mercey B 2007 *J. Magn. Magn. Mater.* **310** 2164
[41] Lee J D and Min B I 1997 *Phys. Rev.* B **55** 12 454
Yu U, Min B I and Lee J D 2000 *Phys. Rev.* B **61** 84
[42] Kim K H, Gu J Y, Choi H S, Park G W and Noh T W 1996 *Phys. Rev. Lett.* **77** 1877
[43] Yoon S, Liu H L, Schollerer G, Cooper S L, Han P D, Payne D A, Cheong S-W and Fisk Z 1998 *Phys. Rev.* B **58** 2795
[44] Prellier W, Haghiri-Gosnet A M, Mercey B, Lecoeur Ph, Hervieu M, Simon Ch and Raveau B 2000 *Appl. Phys. Lett.* **77** 1023
[45] Prellier W, Simon Ch, Haghiri-Gosnet A M, Mercey B and Raveau B 2000 *Phys. Rev.* B **62** R16337
[46] Jirak Z, Krupicka S, Simsa Z, Doulka M and Vratislma S 1985 *J. Magn. Magn. Mater.* **53** 153
[47] Lax M 1978 *Appl. Phys. Lett.* **33** 786
[48] Liarokapis E and Raptis Y S 1985 *J. Appl. Phys.* **57** 5123
[49] Merrill L and Bassett W A 1974 *Rev. Sci. Instrum.* **45** 290
[50] Weinstein B A and Piermarini G J 1975 *Phys. Rev.* B **12** 1172
[51] Martin-Carron L, de Andres A, Martinez-Lope M J, Casais M T and Alonso J A 2002 *Phys. Rev.* B **66** 174303
[52] Iliev M N, Abrashev M V, Lee H-G, Popov V N, Sun Y Y, Thomsen C, Meng R L and Chu C W 1998 *Phys. Rev.* B **57** 2872
[53] Iliev M N, Abrashev M V, Laverdiere J, Jandl S, Gospodinov M M, Wang Y-Q and Sun Y-Y 2006 *Phys. Rev.* B **73** 064302
[54] Xiong Y M, Chen T, Wang G Y, Chen X H, Chen X and Chen C L 2004 *Phys. Rev.* B **70** 094407
[55] Kozlenko D and Savenko B N 2004 *J. Phys.: Condens. Matter* **16** 9031
[56] Hazama H, Goto T, Nemoto Y, Tomioka Y, Asamitsu A and Tokura Y 2004 *Phys. Rev.* B **69** 064406
[57] Samara G A and Giardanini A A 1965 *Phys. Rev.* B **140** A954
[58] Bouvier P and Kreisel J 2002 *J. Phys.: Condens. Matter* **14** 3981
[59] Ulrich C, Anastassakis E, Syassen K, Debernardi A and Cardona M 1997 *Phys. Rev. Lett.* **78** 1283
[60] Liu M S, Bursill L A, Prawer S and Beserman R 2000 *Phys. Rev.* B **61** 3391
[61] Iliev M N and Abrashev M V 2001 *J. Raman Spectrosc.* **32** 805
[62] Radaelli P G, Cox D E, Marezio M and Cheong S W 1997 *Phys. Rev.* B **55** 3015
[63] Huang Q, Lynn J W, Erwin R W, Santoro A, Dender D C, Smolyaninova V N, Ghosh K and Greene R L 2000 *Phys. Rev.* B **61** 8895
[64] Postorino P, Congeduti A, Dore P, Sacchetti A, Gorelli F, Ulivi L, Kumar A and Sarma D D 2003 *Phys. Rev. Lett.* **91** 175501
[65] Mertelj T, Yusupov R, Filippi M, Prellier W and Mihailovic D 2008 *Appl. Phys. Lett.* **93** 042512
[66] Kozlenko D P, Dubrovinsky L S, Goncharenko I N, Savenko B N, Voronin V I, Kiselev E A and Proskurnina N V 2007 *Phys. Rev.* B **75** 104408